

Proton ordering in tetragonal and monoclinic H₂O ice

Fei Yen^{1,2*}, Zhenhua Chi^{1,2}, Adam Berlie^{1†}, Xiaodi Liu¹, Alexander F. Goncharov^{1,3}

¹Key Laboratory for Materials Physics, Institute of Solid State Physics, Hefei Institutes of Physical Sciences, Chinese Academy of Sciences, Hefei 230031, China.

²High Magnetic Field Laboratory, Hefei Institutes of Physical Sciences, Chinese Academy of Sciences, Hefei 230031, China.

³Geophysical Laboratory, Carnegie Institution of Washington, 5251 Broad Branch Road, NW, Washington D.C., 20015, USA.

Abstract: H₂O ice remains one of the most enigmatic materials as its phase diagram reveals up to sixteen solid phases. While the crystal structure of these phases has been determined, the phase boundaries and mechanisms of formation of the proton-ordered phases remain unclear. From high precision measurements of the complex dielectric constant, we probe directly the degree of ordering of the protons in H₂O tetragonal ice III and monoclinic ice V down to 80 K. A broadened first-order phase transition is found to occur near 202 K we attribute to a quenched disorder of the protons which causes a continuous disordering of the protons during cooling and metastable behavior. At 126 K the protons in ice III become fully ordered, and for the case of ice V becoming fully ordered at 113 K forming ice XIII. Two triple points are proposed to exist: one at 0.35 GPa and 126 K where ices III, IX and V coexist; and another at 0.35 GPa and 113 K where ices V, IX and XIII coexist. Our findings unravel the underlying mechanism driving the continuous proton ordering in H₂O ice and reveal how the phase diagram of H₂O is far more complex than previously thought.

PACS numbers: 64.60.Cn, 64.70.K-, 77.22.-d, 77.22.Gm

The sixteen solid phases of H₂O are classified according to their crystalline structure and whether their hydrogen bonds are in an ordered or disordered configuration. With H₂O being the most abundant solid in our universe, with vast quantities existing right here on Earth and within our solar system, ice researchers across the board are in need of knowing the structures, processes and patterns that the different ice phases exhibit [1]. The crystal structures of most ice phases have already been resolved but not their kinetic processes. Much of the complexities in ice arise from intra and intermolecular bonding of the hydrogen atoms [2]. However, a complete picture of when the protons governing the hydrogen bonds order, disorder, or partially order is not yet available.

In H₂O ice each hydrogen atom is linked to two oxygen atoms: one as an intramolecular covalent bond (H-O-H) and another as an intermolecular hydrogen bond (H₂O···HOH). Each oxygen atom is linked to four hydrogen atoms: two as covalent bonds and two as hydrogen bonds [3]. The position of the hydrogen proton is closer to the covalent bonded oxygen so each proton can rest in one of two possible sites. Ice structures can be regarded as being made up of tetrahedral arrangements of oxygens with four hydrogens within. The protons inside each tetrahedra can arrange into six distinct configurations (Fig. 1). The proton ordered state refers to each tetrahedra having the same proton configuration globally and the disordered state when the proton configuration of the tetrahedras are random. The protons are usually disordered near the liquidus line due to thermal excitations whilst becoming completely ordered at lower temperature. At temperatures in between, the transitioning between the proton ordered and disordered states is still not well understood.

H₂O in the pressure range $0.21 < P < 0.35$ GPa crystallizes in the tetragonal structured (space group P4₁2₁2) ice III phase [4] (Fig. 2). At temperature $T < 244$ K, ice III transforms into rhombohedral structured ice II (space group R3 [5]). At $T < 173$ K, any residual ice III that did not transform into ice II is believed to transform into ice IX [7], the proton ordered form of ice III. The formation of ice IX is complicated as the proton ordering process is continuous starting from ~4% ordered ice III to ~96% ordered ice IX upon cooling [4,6,7]. The warming process on the other hand, has not been studied in detail, of which we investigate in part in this work.

In the range of $0.35 < P < 0.62$ GPa, H₂O crystallizes into a monoclinic structured ice V phase [8]. At lower temperature, ice V also transforms into ice II. Alike ice III, ice V which is also mostly proton disordered [9], also has a proton ordered phase ice XIII [10]. The formation process of ice XIII is still unclear and a detailed study of the proton dynamics between ices V and XIII has never been performed until this work.

To obtain a clearer picture of the extent at which the protons order under different pressure and temperature, the study of a response function sensitive to changes in the intermolecular bonds is needed [11]. For this reason, we carried out high precision measurements of the complex dielectric constant on millimeter-sized crystalline samples of H₂O as a function of temperature up to 0.76 GPa. In this Letter, we present a detailed study on two isobars at 0.31 and 0.59 GPa to understand the proton dynamics in tetragonal and monoclinic ices and discuss the implications it has on the phase diagram.

The samples were prepared by pressurizing de-ionized, liquid H₂O (Milli-Q Direct 8) to the desired pressure at room temperature with a BeCu clamp cell and then cooled to 77 K at 3-5 K/min via a customized gas exchange cryostat. The real and imaginary parts of the dielectric constant were obtained by measuring the capacitance and loss tangent, respectively, of a pair of Pt electrodes in the form of parallel plates at 1 kHz with an Andeen Hagerle (AH2500A) capacitance bridge. The electrodes were dipped inside a Teflon capsule filled with liquid H₂O so the sample itself was also the pressure medium. Force was applied only when the sample was in liquid form so a large crystal (ϕ 4 mm by 9 mm) free of shear stresses was obtained upon freezing. Warming speeds were 1–2 K/min [12]. Pressure was deduced from the melting of H₂O indicated by the increase of the response functions by a few orders of magnitude.

Fig. 3(a) shows the real part of the dielectric constant $\epsilon'(T)$ at 0.31 GPa with the inset showing the imaginary part $\epsilon''(T)$. At $T_{L_III+SCW}=252$ K during cooling, part of the sample transformed into ice III represented by a shoulder type discontinuity in $\epsilon'(T)$ and $\epsilon''(T)$ coinciding exactly with the H₂O liquidus line [13]. The residual liquid that did not transform remained as supercooled water (SCW) until $T_{III+SCW_III+II}=232$ K where the SCW transformed into ice II marked by a sharp drop in both $\epsilon'(T)$ and $\epsilon''(T)$. From this point, the sample was composed of a mixture of ices II and III. In the range of $211 > T > 164$ K, $\epsilon'(T)$ decreased by over half its value and $\epsilon''(T)$ exhibited a minimum at 211 K and a maximum at 202 K. The dielectric constant within an ice phase usually does not change by much so the origin of such drastic change can only stem from proton ordering dynamics. Since the protons in ice II are already ordered, the only protons left to become ordered are those in ice III. Indeed, Whalley et al. [7] concluded that continuous proton ordering occurs in ice III from 208 K to 163 K to end up forming ice IX.

It was later confirmed by neutron diffraction on D₂O [4,6] that only 96% of the deuterons ordered at ~ 77 K. According to Ref. [14], the protons should undergo a first-order phase transition to become a fully ordered antiferroelectric ground state at 126 K from DFT calculations. Unfortunately, Whalley et al., [7] only presented data down to 158 K and the neutron diffraction studies were not carried out *in situ* and on a hydrostatic stress-free sample. With our stress-free samples, we were able to observe the expected phase transition at 126 K in the form of a change of slope discontinuity in $d\epsilon''(T)/dT$ [Fig. 3(c)]. This suggests that the phase transition line bounding ice IX should actually be drawn at $T_{IX_III}=126$ K, (when full proton order is achieved) instead of near 173 K (when only $\sim 96\%$ has been achieved) as shown in most literature.

During warming, both $\epsilon'(T)$ and $\epsilon''(T)$ took a different path from their cooling curves starting from $T > 164$ K. A peak anomaly was observed in $\epsilon'(T)$ and $\epsilon''(T)$ at $T_m = 202$ K with an onset near 183 K and offset at $T_m' = 211$ K [dashed line in Fig. 3(b)]. T_m and T_m' were also observed as a minimum and maximum in $\epsilon''(T)$ during cooling, though with a higher magnitude and less pronounced. In the $\epsilon'(T)$ curve during cooling, T_m' was not observed, but T_m coincided with the beginning of the ordering of the protons. T_m appears to be a first-order phase transition experiencing kinetic broadening due to the presence of microscopic inhomogeneities usually caused by defects or impurities [15]. We believe that proton disorder is also a type of quenched disorder that causes local inhomogeneities since the lattice periodicity is distorted by the randomness of the proton configuration in each tetrahedra. This inhibits long range order which causes the protons to require a finite temperature range to order ($211 > T > 164$ K). Large hysteretic regions also usually accompany systems with quenched disorder which also explains the differences observed between the warming and cooling curves.

Upon further warming, the values of $\epsilon'(T)$ and $\epsilon''(T)$ remained lower than their respective values during cooling when $T > T_m'$, indicating that the protons in the ice III phase are in a more ordered state during warming. At $T_{II_III} = 245$ K, an expected anomaly due to the ice II/III phase line was observed in the form of a sharp step.

Figure 4 shows $\epsilon'(T)$ and $\epsilon''(T)$ at 0.59 GPa. The sample persisted as SCW down to $T_{SCW_V} = 252$ K where it transitioned into ice V indicated by a sharp drop in both $\epsilon'(T)$ [Fig. 4(a)] and $\epsilon''(T)$ [Fig. 4(b)]. Upon further cooling, a shoulder type anomaly was observed at $T_{V_II} = 214$ K where $\epsilon'(T)$ began to decrease by 60% before saturating near 170 K [inset of Fig. 4(a)]. Again, $\epsilon''(T)$ should not change much when it is in the same phase so such drastic changes can only be attributed to a continuous ordering of the protons alike the case in ice III. Since the protons in ice II are supposed to be ordered, this suggests that not only ice II is present but also a residual mixture of ice V. This is confirmed by the presence of a discontinuity in the form of a change in linear to non-linear behavior at $T_{XIII_V} = 113$ K in $d\epsilon''(T)/dT$ at 0.38 and 0.59 GPa [Fig. 4(c)]. Salzmann et al. observed a reversible phase transition between ices V and its ground state ice XIII at 112 K, though at ambient pressure after subjecting the sample to 0.50 GPa via differential calorimetric measurements [16]. Here, T_{XIII_V} was observed *in situ* and can only be attributed to the ice XIII/V transition of any residual ice that did not transform into ice II. This calls for the phase diagram to also include a phase line bounding ice XIII starting from 0.35 GPa. With a large difference in entropy between

ice V and a fully ordered ice XIII along with a small change in volume during the phase transition, the T_{XIII_V} phase line should be nearly temperature independent according to the Clausius-Clapeyron (dashed line at 113 K in Fig. 2).

Upon warming, T_m and T_m' were also observed in $\epsilon'(T)$ at 0.59 GPa. T_m' was masked by the ice II/V transition line which shows up as minima in $\epsilon''(T)$ at $T_{V_{II}}=214$ K and $T_{II_V}=219$ K. The differences in magnitude between cooling and warming indicate that the protons are also in a more ordered state during warming in monoclinic ice suggesting how metastable behavior within the ice phases can be pinpointed to originate from quenched proton disorder.

T_m was observed in the pressure region of $0.07 < P < 0.59$ GPa (Fig. 5) drawn as a dashed curve in Fig. 2. At 0.76 GPa, T_m and T_m' were no longer visible since ice VI exists in this part of the phase diagram [9]. Interestingly, T_m and T_m' were also no longer detected at 0.05 GPa which provides compounding evidence that a second critical point exists in this part of the phase diagram as predicted by many [17,18]. The T_m phase line covers the tetragonal and monoclinic ices in its entirety suggesting that the associated proton ordering dynamics is more correlated to thermal energy than a consequence of crystal structure.

From piston displacement isothermals up to 0.65 GPa, Bauer et al., were able to obtain pure ice II, pure ice III, or an ice II/III mixture depending on the compression rate [19]. Their phase transition into the ice II phase space was density-driven forming from ice Ih, whereas ours' was temperature-driven forming from liquid H₂O and ice III. A larger percentage of ice III with a limited amount of ice II can also be obtained if the sample is quenched [4]. This shows how the ice II/III ratio is dependent on T , ΔT , P , and ΔP , which can be of great use in deciphering the history of any ice found in environments that lie in the ice II phase space. Suppose now that liquid H₂O was suddenly quenched to 77 K at 0.35 GPa so formation of ice II was greatly suppressed, then upon warming, a triple point would exist at 0.35 GPa and 113 K where ices V, IX and XIII coexist (blue circle in Fig. 2). At slightly higher temperature, another triple point should also exist at 0.35 GPa and 126 K where ices III, V and IX coexist.

In summary, a first-order phase transition T_m with kinetic broadening was identified near 202 K extending from 0.07 to 0.62 GPa. We attribute the broadening of T_m to the quenched disorder of the protons which results in a continuous disorder of the protons and metastable behavior. Full proton ordering was identified at 125 and 113 K in tetragonal and monoclinic ice, respectively. The existing H₂O phase diagram

needs to be slightly modified by: lowering the phase line bounding ice IX from 173 K to 126 K; drawing another phase line bounding ice XIII at 113 K starting from 0.35 GPa; and taking into consideration the existence of two new triple points.

ACKNOWLEDGEMENTS

This work was made possible in part via the support of the National Science Foundation of China grants No. 11374307, No. 51372249, and the Director Grants of Hefei Institute of Physical Sciences, Chinese Academy of Sciences (CASHIPS).

REFERENCES

*fyen@issp.ac.cn

†Present address: Research School of Chemistry, Australian National University, Canberra, 0200, Australia

1. Bartels-Rausch, T., et al. Ice structures, patterns, and processes: A view across the icefields. *Rev. Mod. Phys.* **84**, 885 (2012).
2. Stokely K., Mazzaa, M. G., Stanley, H. E., Franzese, G. Effect of hydrogen bond cooperativity on the behavior of water. *Proc. Nat. Acad. Sci.* **107**, 1301-1306 (2010).
3. Bernal, J. D., Fowler, R. H. A theory of water and ionic solution, with particular reference to hydrogen and hydroxyl ions. *J Chem. Phys.* **1**, 8, 515 (1933).
4. Londono, J. D., Kuhs, W. F., Finney, J. L. Neutron diffraction studies of ices III and IX on under-pressure and recovered samples. *J. Chem. Phys.* **98**, 4878-4888 (1993).
5. Kamb, B. Ice II: A proton-ordered form of ice. *Acta Crystallogr.* **17** 1437-1449 (1964).
6. La-Placa, S. J., Hamilton, W. C., Kamb, B., Prakash, A. On a nearly proton-ordered structure for ice IX. *J. Chem. Phys.* **58**, 567-580 (1973).
7. Whalley, E., Heath, J. B. R., Davidson, D. W. Ice IX: An antiferroelectric phase related to Ice III*. *J. Chem. Phys.* **48**, 5, 2362 (1968).
8. Kamb, B., Prakash, A., Knobler, C. Structure of ice V. *Acta Crystallogr.* **22** 706-715 (1967).
9. Lobban, C., Finney, J. L., Kuhs, W. F. The structure of a new phase of ice. *Nature* **391**, 268 (1998).
10. Salzmann C. G., Radaelli, P. G., Hallbrucker, A., Mayer E., Finney, J. L. The preparation and structures of hydrogen ordered phases of ice. *Science* **311**, 1758 (2006).
11. Since an equivalent dipole moment exists for each hydrogen bond, $p=q\mathbf{l}$, where q is the elemental charge and \mathbf{l} an equivalent distance between the hydrogen proton and

surrounding oxygen, any shift in I will also change the macroscopic polarization, hence the dielectric constant. The imaginary part of the dielectric constant, essentially the loss factor, should even be more sensitive since the protons progressively become more rigid as they become more ordered.

12. With this method, only a partial percentile of an ice phase undergoing a phase transition or proton ordering can be detected as long as the rest of the ice mixture remains static since we are looking at changes of the charge distribution, not still frames such as diffraction and spectroscopy which require a larger percentage of the sample to be in a singular phase.

13. Bridgman, P. W. Water, in the liquid and five solid forms, under pressure. *Proc. Am. Acad. Arts Sci.* **47**, 439-558 (1912).

14. Knight, C., Singer, S. J. A reexamination of the ice III/IX hydrogen bond ordering phase transition. *J. Chem. Phys.* **125**, 064506 (2006).

15. Imry, Y., Wortis, M. Influence of quenched impurities on first-order phase transitions. *Phys. Rev. B* **19**, 3580 (1979).

16. Salzmann, C. G., Radaelli, P. G., Finney, J. L., Mayer, E. A calorimetric study on the low temperature dynamics of doped ice V and its reversible phase transition to hydrogen ordered ice XIII. *Phys. Chem. Chem. Phys.* **10**, 6313 (2008).

17. Mishima, O. Volume of supercooled water under pressure and the liquid-liquid critical point. *J. Chem. Phys.* **133**, 144503 (2010).

18. Chiu, J., Starr, F. W., Giovambattista, N. Heating-induced glass-glass and glass-liquid transformations in computer simulations of water. *J. Chem. Phys.* **140**, 114504 (2014).

19. Bauer, M., Elsaesser, M. S., Winkel, K., Mayer, E., Loerting, T. Compression-rate dependence of the phase transition from hexagonal ice to ice II and/or ice III. *Phys. Rev. B* **77**, 220105R (2008).

FIGURES

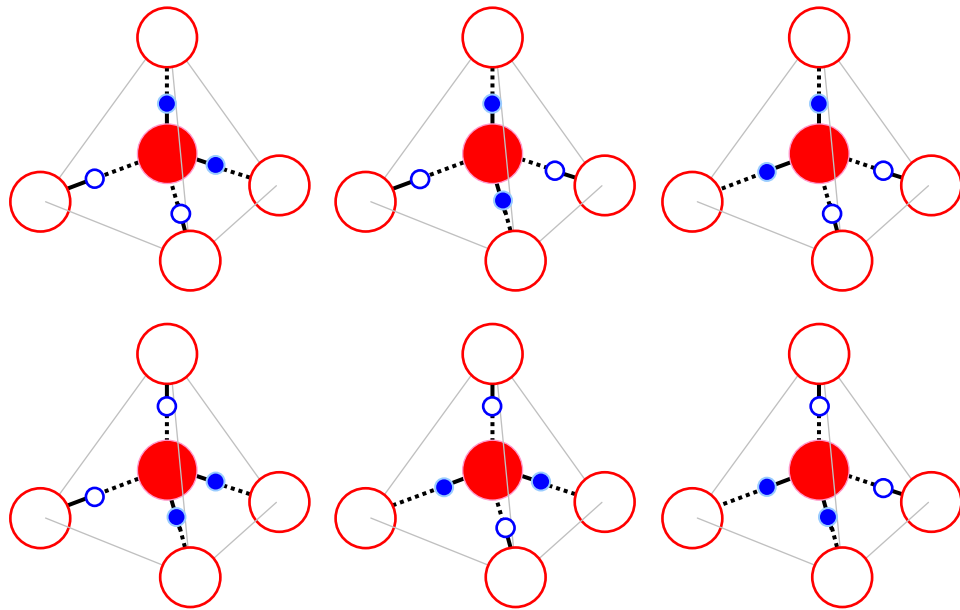


FIG. 1 (color online). All ice structures including tetragonal and monoclinic ice are composed of an arrangement of H_4O_2 tetrahedra of which six possible configurations can take place. Red (blue) spheres are oxygen (hydrogen) atoms. Each hydrogen possess a hydrogen bond (\cdots) and a covalent bond (—) to two oxygen. The H_2O molecule resides fully inside the tetrahedron depicted in solid colors.

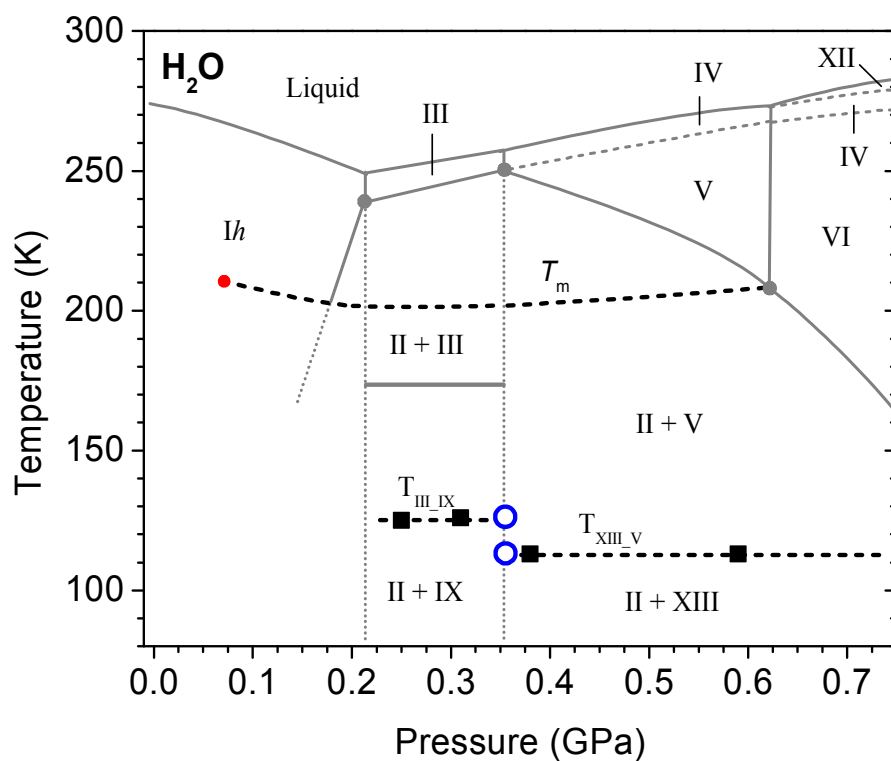


FIG. 2 (color online). Phase diagram of H₂O ice. Since ices III, V, IX and XIII may exist in metastable form in the phase space of ice II, a mixture of ice II may also be present indicated by a “+” sign. Dashed black lines are phase lines related to proton dynamics derived from this work. Dashed grey lines are phase lines bounding metastable phases. T_m is a first-order phase transition related to proton disordering spanning from 0.07 to 0.62 GPa. T_{III_IX} and T_{XIII_V} are the temperatures when the protons in ice III and V, respectively, become fully ordered forming ices IX and XIII. Blue circles represent two triple points: one at 0.35 GPa and 126 K where ices III, V and IX coexist; and another at 0.35 GPa and 113 K where ices V, IX and XIII coexist.

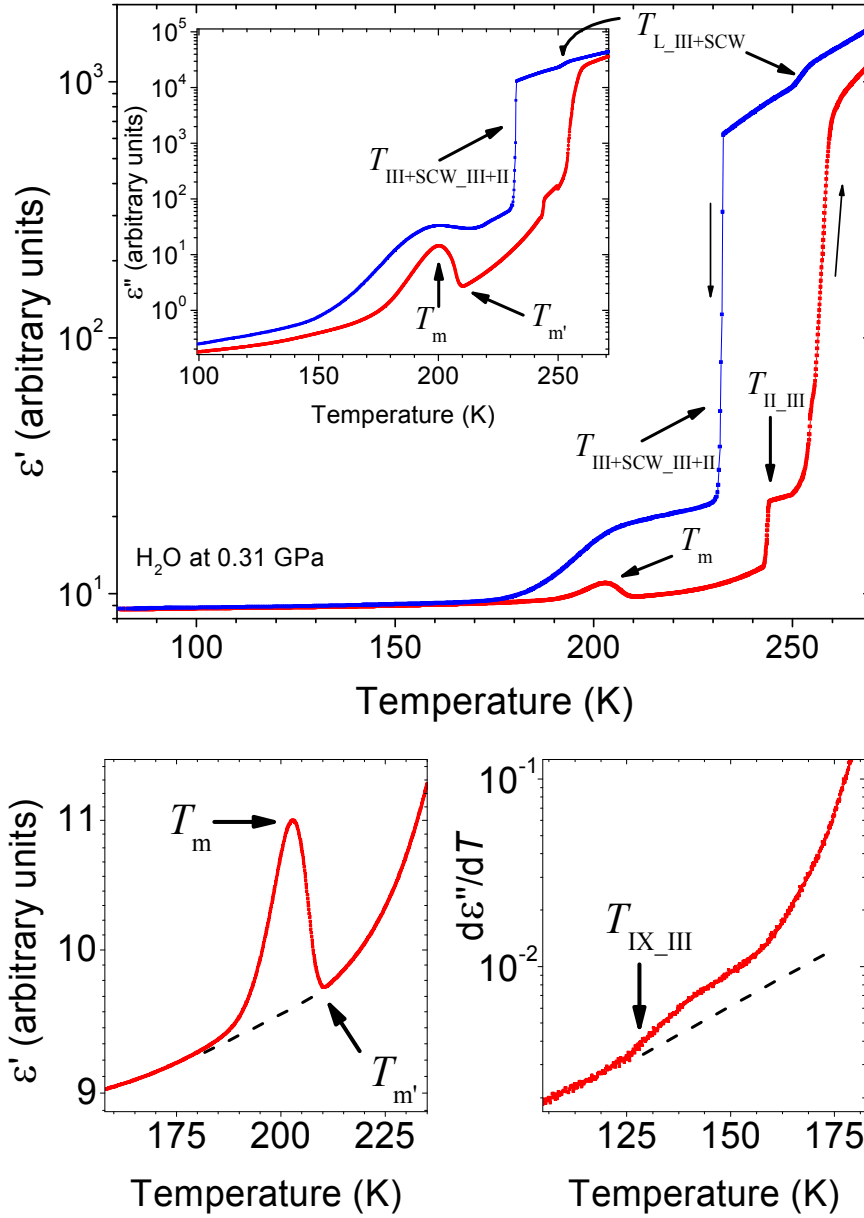


FIG. 3 (color online). (a) Real $\epsilon'(T)$ and imaginary $\epsilon''(T)$ (inset) parts of the dielectric constant. At $T_{L_III+SCW}=254$ K, part of the sample transformed into ice III while the rest remained as supercooled water (SCW). At $T_{III+SCW_III+II}=232$ K, the remaining SCW transformed into ice II forming a mixture of ices II and III. (b) First-order phase transition at $T_m=202$ K experiencing kinetic broadening with an onset at ~ 173 K and offset at $T_{m'}=212$ K. The broadening of T_m is attributed to the presence of quenched proton disorder in ice III which yields microscopic inhomogeneities inhibiting long range order. Consequently, the protons in ice III require a finite range of temperature to order during cooling ($208 < T < 164$ K); and large metastable and hysteretic regions exist. At $T_{II_III}=244$ K, the system enters into the phase space of ice III. (c) An anomaly in the form of a linear to nonlinear change in $d\epsilon''(T)/dT$ at $T_{IX_III}=126$ K attributed to the full ordering of the protons after Knight et al. [14].

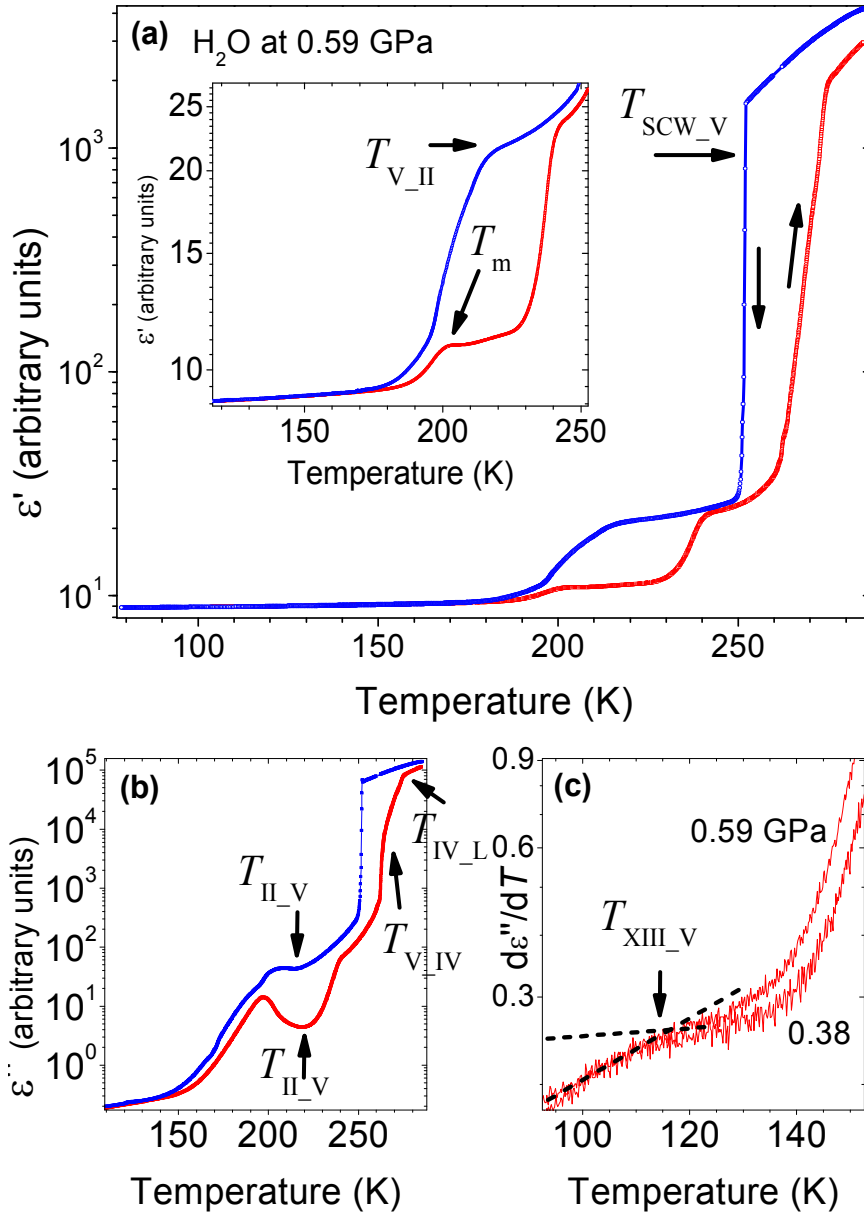


FIG. 4 (color online). (a) $\epsilon'(T)$ at 0.59 GPa. SCW persisted down to $T_{\text{SCW}_V}=252$ K where it solidified into ice V. At $T_{V_{\text{II}}}=214$ K (inset), most of the ice V transformed into ice II with some residual ice V remaining. Alike tetragonal ice, T_m and T_m' were also observed in monoclinic ice along with continuous proton disordering and large hysteretic regions. (b) $\epsilon''(T)$ at 0.59 GPa. The reversible ice II/V transitions appear as minima at $T_{\text{II}_V}=219$ K and $T_{V_{\text{II}}}=214$ K. Before melting, transformation of ice V into metastable ice IV was also evident at $T_{V_{\text{IV}}}$. (c) $d\epsilon''(T)/dT$ at 0.38 and 0.59 GPa. Anomaly at $T_{\text{XIII}_V}=113$ K is attributed to the phase transition of fully ordered ice XIII to ice V.

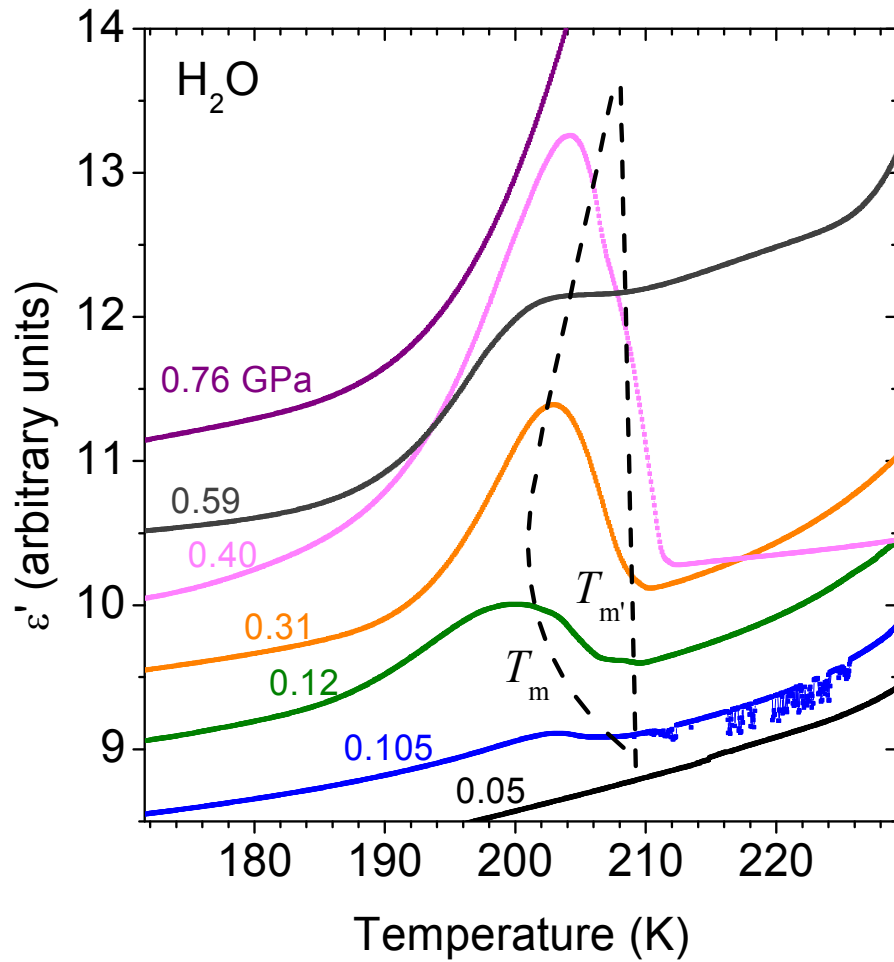


FIG. 5 (color online). Pressure dependence of T_m and $T_{m'}$. The continuous behavior of T_m spanning through $0.07 < P < 0.62$ GPa suggests that the associated proton ordering dynamics is not strictly a consequence of crystal structure but instead dependent more on thermal energy. The 0.105 and 0.400 isobars were from a different sample.